Clinical Radiology 74 (2019) 978.e9–978.e14

Contents lists available at ScienceDirect

Clinical Radiology

journal homepage: www.clinicalradiologyonline.net

Feasibility of three-dimensional constructive interference in steady state sequences for evaluating the anterolateral ligament

Y. Zhu [a,1], X. Qiu [b,1], T. Yu [c,**], C. Zhang [a], X. Zhao [a], F. Duan [a], D. Hao [a,*]

[a] Department of Radiology, The Affiliated Hospital of Qingdao University, Qingdao, 266003, China
[b] Department of Radiology, Beijing Friendship Hospital, Capital Medical University, Beijing, 100050, China
[c] Department of Sport Medicine, The Affiliated Hospital of Qingdao University, Qingdao, 266003, China

ARTICLE INFORMATION

Article history:
Received 12 April 2019
Accepted 20 August 2019

AIM: The purpose of the study was to determine the feasibility of three-dimensional (3D) constructive interference in steady state (CISS) sequences for evaluating the anterolateral ligament (ALL).

MATERIALS AND METHODS: Magnetic resonance imaging (MRI) of the right knee joint in 30 healthy volunteers was performed using a 3 T MRI machine. Axial T2-weighted imaging with fat saturation (T2WI-FS), coronal proton-density-weighted imaging with fat saturation (PDWI-FS), and 3D-CISS were included in the protocol. Multiplanar reconstruction (MPR) and rotating stretched curved planar reconstructions (CPRs) of the ALL at 30°, 60°, 90°, 120°, and 150° were generated from the 3D-CISS images. The visibility of the femoral part, meniscal part, tibial part, meniscal insertion, femoral footprint, and tibial footprint of the ALL on the imaging of all sequences was recorded.

RESULTS: Based on the CPR of 3D-CISS MRI, the presence of tibial and femoral footprints of the ALL was rated superior to MPR and PDWI-FS (96.67% and 96.67%, respectively; $p<0.017$). Rotating CPR of 3D-CISS MRI imaging was rated superior to PDWI-FS with respect to the tibial part, meniscal part, and meniscal insertion of the ALL (96.67%, 83.33%, and 83.33%, respectively; $p<0.05$). Rotating CPR of 3D-CISS MRI was rated superior to PDWI-FS with respect to the femoral part of the ALL, but the difference was not statistically significant ($p=0.095$). The angle between the ALL and lateral collateral ligament (LCL) on the oblique sagittal image was 18.34±1.88°.

CONCLUSIONS: The MRI 3D-CISS sequences significantly enhanced the ability to identify the ALL compared to the 2D MRI sequences.

* Guarantor and correspondent: DaPeng Hao, Department of Radiology, The Affiliated Hospital of Qingdao University, 16, Jiangsu Road, Qingdao, 266003, China. Tel.: +86 18661802582.
** Guarantor and correspondent: T. Yu, Department of Sport Medicine, The Affiliated Hospital of Qingdao University, 16, Jiangsu Road, Qingdao, 266003, China. Tel.: +86 18661808912.
E-mail addresses: qiuxy520@163.com (X. Qiu), ytb8912@163.com (T. Yu), haodp__2009@163.com (D. Hao).
[1] These authors contributed to the work equally and should be regarded as co-first authors.

https://doi.org/10.1016/j.crad.2019.08.014
0009-9260/

Introduction

The ligamentous anatomy of the knee joint has been studied extensively and clearly defined. Recently, the anatomy of the lateral ligamentous complex of the knee joint has been a focus of many studies.[1] The anterolateral ligament (ALL) is one of these ligaments. Segond first mentioned the ALL in the orthopaedic literature in 1879. Segond described a constant avulsion fracture pattern involving the anterolateral proximal tibia as a result of forced internal rotation at the knee joint. In 2007, Vieira *et al.* named the structure the anterolateral ligament (ALL).[2] Most studies[3–5] have used routine two-dimensional (2D) sequences to evaluate the ALL; however, the results have not been consistent. Klontzas *et al.*[6] used multiplanar reconstruction (MPR) of three-dimensional (3D)-constructive interference in steady state (CISS) magnetic resonance imaging (MRI) sequences to evaluate the ALL. The study illuminated the relationship between the ALL and the lateral collateral ligament (LCL), but detailed imaging features were not described.

In the present study it was hypothesised that 3D-CISS sequences imaging at 3 T has the same or superior diagnostic performance compared to 2D sequences in evaluating the ALL. The purpose of the present study was to determine the feasibility of 3D-CISS MRI sequences for evaluating the ALL.

Materials and methods

Patients

In the present study a total of 30 volunteers (20 males and 10 females) were selected. The mean age was 26.5±2.8 years (range, 24–36 years). The mean weight was 65±9.39 kg (range, 50–85 kg) and the mean height was 171.5±6.07 cm (range, 162–185 cm). Patients with a history of open knee surgery, knee arthroscopy, knee trauma, and tumours of the lateral compartment of the knee were excluded from the study. This study was approved by the Ethics Committee of the hospital. The experimental design fully considered the principles of safety and fairness, and the research content did not cause harm or risk to the volunteers. Volunteer recruitment was based on the principle of voluntary and informed consent. There were no conflicts of interest between the content and research findings.

MRI protocol

MRI examinations were performed using a Siemens Magnetom Skyra 3 T MRI system (Siemens, Erlangen, Germany) using a dedicated knee coil (HD T/R eight-channel high resolution knee array). The protocol included coronal proton-density-weighted (PDW) fast spin-echo (FSE) sequences with fat saturation (FS), axial T2-weighted sequences with FS, and 3D-CISS sequences. The parameters are described in Table 1.

Image analyses

Visualisation of every part of the ALL or the complete structure on coronal 2D MRI images and 3D-CISS high-resolution images was analysed as a dichotomous variable (yes or no). Regarding the 3D-CISS high-resolution sequences, the Siemens workstation was used to obtain the reconstructed images (MRP and rotating curve planar reconstruction [rotating CPR]). According to MPR, an oblique coronal plane parallel to the ALL, an oblique sagittal plane crossing through the proximal attachment, and a transverse plane perpendicular to the sagittal plane were used. The method used to visualise structures with a small diameter was to re-sample and visualise the data set according to the high-level information gained from the centreline detection process; this process is referred to as CPR. Rotating the longitudinal section around the central axis provides an opportunity to inspect the entire ligament. A stretched rotating CPR was generated by rotating the vector-of-interest around a pre-defined axis. The rotating CPR was rotated by changing the angle-of-interest accordingly. The rotating CPR of the ALL at 30°, 60°, 90°, 120°, and 150° was generated from images of 3D-CISS sequences (Figs 1 and 2).

The presence of a femoral footprint, tibial footprint, and the meniscal insertion of the ALL on 2D MRI images and 3D-CISS MRI images (MPR and rotating CPR) were also recorded. The angle of the LCL and straight line from origin-to-insertion of the ALL was recorded on the images of the MPR.

Two experienced musculoskeletal radiologists (12 and 10 years of experience) evaluated the MRI examinations independently using all imaging planes on the PACS. The 2D and 3D-CISS images from each volunteer were randomly presented.

Statistical analysis

To compare the visibility frequency of the ALL in each part and section, the existence of a marginal association was examined using a χ^2 test. The difference was statistically significant ($p<0.05$), and the difference between the two groups was statistically significant for the difference ($p<0.017$).

Results

The coronal images of CPR clearly showed the direction of the ALL fibres, showing a thin linear structure starting from the lateral femoral condyle and coursing obliquely downward and forward, inserting in the lateral meniscus and attaching to the lateral aspect of the proximal tibia between Gerdy's tubercle and the tip of fibular head (Fig 3). On the coronal images of the CPR, the ALL is divided into three parts (femoral, meniscal, and tibial parts). The meniscal insertion, femoral footprint, and tibial footprint of the ALL can be displayed easily (Fig 2b–e). In the oblique sagittal images of the MPR, the common origin of the ALL and LCL, as well as the tibial attachment point of the ALL,

Table 1
Imaging parameters of two-dimensional (2D) sequences and constructive interference in steady state (CISS) sequence at 3 T.

Sequence	TR (ms)	TE (ms)	Matrix	FOV (mm×mm)	ST (mm)	Spacing (mm)	NEX	Time
Coronal PDW FS	2600	33	320×272	170×170	4.0	0.8	1	1 min 39 s
Axial T2W FS	5250	92	320×272	150×150	4.0	0.8	1	2 min 18 s
CISS	8.56	3.91	320×307	150×150	0.5	0.1	1	6 min 51 s

TR, repetition time; TE, echo time; FOV, field of view; ST, Slice thickness; NEX, number of excitations; PDW, proton-density weighted; FS, fat saturation; T2W, T2-weighted.

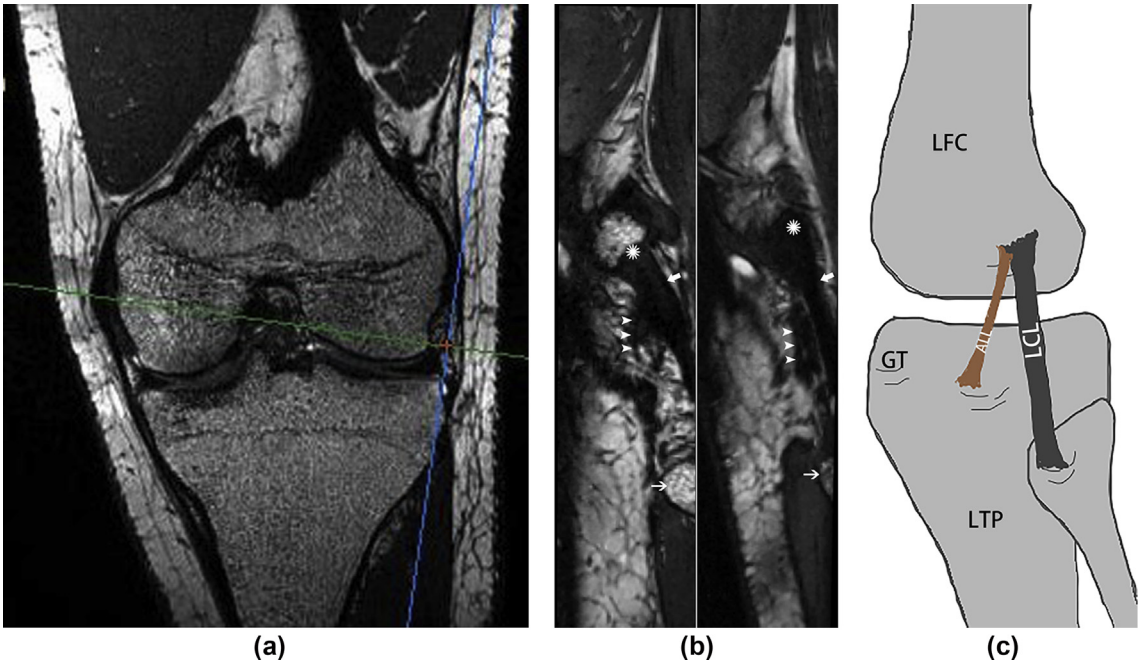

Figure 1 Imaging of 3D-CISS with MPR (a, b) and schematic drawing (c). (a) Positioning image. The blue line is the positioning line of the oblique sagittal plane. (b) Oblique sagittal images of two volunteers, 28-year-old man and 24-year-old woman. The ALL is shown anteriorly (arrowheads), lateral collateral ligament (LCL) posteriorly (thick arrow), and the common footprint superiorly (white asterisk). The head of the fibula is shown (arrow). LFC, lateral femoral condyle; LTP, lateral tibial plafond; GT, Gerdy's tubercle.

were clearly visualised (Fig 1b). The angle between the ALL and LCL was 18.34±1.88° (range, 13.5–21°).

On the PDW FS images, the ALL appears as a linear low-signal shadow, which is attached to the lateral femoral condyle, superior border of the lateral meniscus, and the lateral surface of the tibia. The lateral genicular artery and vein are visible on the inner side of the ALL, and the LCL and iliotibial band are visible on the lateral side surrounded by fatty tissue (Fig 3).

The visibility of each portion and insertion of the ALL on MPR and CPR images of the 3D-CISS sequences and PDW FS images are shown in Table 2. In the three groups of images, the visibility of the CPR was higher than the MPR and PDW FS for the tibial and femoral attachment points. For the tibial footprint and femoral footprint, there was no statistical significance (p=0.554) for visibility of the CPR and MPR images; there was statistical significance (p<0.017) for the visibility of CPR, MPR, and PDW FS images. For the femoral footprint, the conditions were the same. The visibilities of the tibial portion, meniscal portion, and the meniscal insertion on the CPR images of the 3D-CISS sequences were higher than PDW FS; the difference was statistically significant (p=0.023, p=0.024, and p=0.006, respectively).

Discussion

As a ligamentous structure of the lateral knee compartment, the ALL has aroused the interest of researchers. Until 2013, few reports had studied the anatomical and imaging features of the ALL. Since that time, many researchers have studied the ALL, including the anatomy, biomechanics, and the presence of each part and relationship with adjacent structures. Helito *et al.*[5,7,8] demonstrated the meniscal insertion of the ALL based on anatomy and imaging. ALL insertion occurred macroscopically in the transition between the anterior horn and the body of the lateral meniscus. Van Dyck *et al.*[9] demonstrated that the ALL injuries were highly associated with lateral meniscal injuries by retrospectively identifying images of acute anterior cruciate ligament (ACL) rupture and injuries. Macchi *et al.*[10] showed in a cadaveric dissection study that the femoral origin of the ALL is somewhat variable in position. This

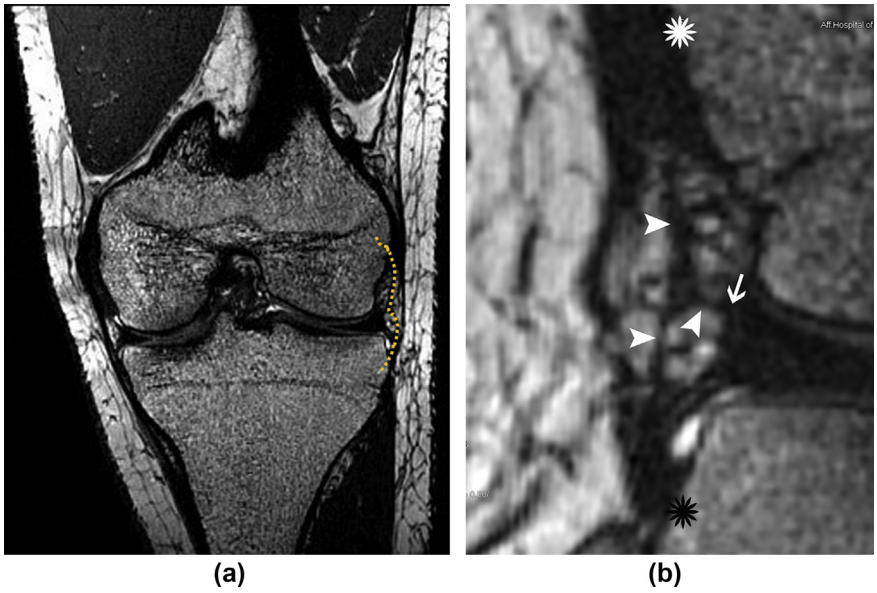

Figure 2 3D-CISS with CPR imaging of a 27-year-old man. (a) Curve along the femoral footprint, the ALL, and the tibial footprint. (b) CPR imaging. The ALL is shown clearly (arrowheads), including the femoral, meniscal, and tibial portions. The meniscal insertion of the ALL is shown clearly (arrow). The origin point (white asterisk) and tibial insertion (black asterisk) are shown clearly.

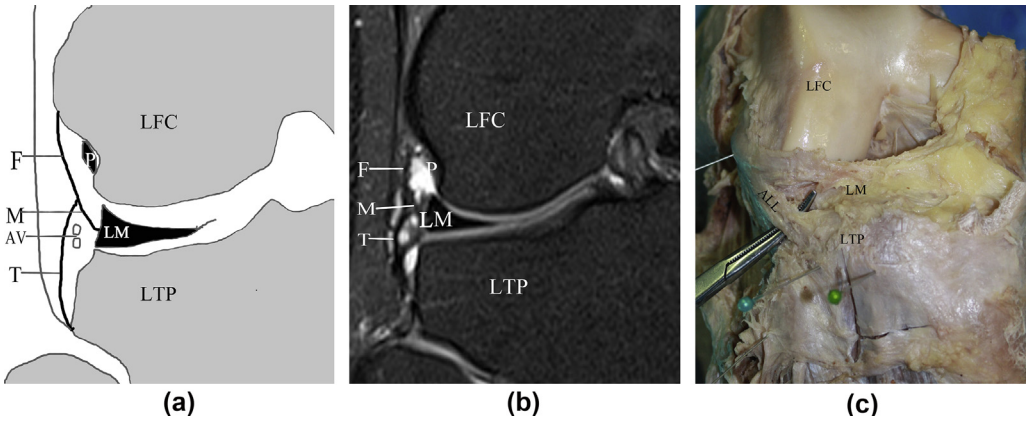

Figure 3 (a) Schematic drawing, (b) coronal PD-weighted MRI with fat suppression, and (c) an anatomical photograph showing the ALL, its origin and insertion, and its relationship to adjacent structures. LFC, lateral femoral condyle; LTP, lateral tibial plafond; LM, lateral meniscus; P, popliteus tendon; AV, inferior lateral genicular artery and vein; F, anterolateral ligament femoral portion; M, anterolateral ligament meniscal portion; T, anterolateral ligament tibial portion.

origin inserts either posterior–proximal or anterior–distal to the femoral origin of the LCL.

Anatomical and imaging studies involving the visibility of the ALL are common. Anatomical studies have shown the high visibility of the ALL in cadavers, ranging from 83–100%,[11–15] while imaging studies range from 51–100%.[4,5,8–10,16–18] Van Dyck *et al.*[9] reported rates of 100% in an imaging study. Kosy *et al.*[3] showed that the visibility of the femoral, meniscal, and tibial parts of the ALL was 59%, 94%, and 94% on PDW imaging, respectively. Helito *et al.*[8] showed that the visibility of the femoral, meniscal, and tibial parts of the ALL was 69.6%, 75.7%, and 39.3% on T2W FS imaging, respectively. Macchi *et al.*[10] showed that the visibility of the femoral, meniscal, and tibial parts of the ALL was 80%, 66%, and 80% on T1W and T2W FS imaging, respectively. In the current study, the visibility of the femoral, meniscal, and tibial parts of the ALL on PDW FS imaging was 73.3%, 56.7%, and 76.7%, respectively. There was an obvious discrepancy regarding visibility between the current study and previous reports because of the quality of imaging, position of the knee, and experience of the radiologists. The visibility of the meniscal insertion, femoral footprint, and tibial footprint of the ALL on 2D MRI was 50%, 16.7%, and 66.7%, respectively. The visibility of the femoral footprint was low because the ALL and LCL femur attachment points had a common starting point; the attachment points were very close and difficult to distinguish.

Along with the development of imaging technology, research on ALL fine anatomy, high-resolution imaging, and

Table 2
Number of views and percentage viewing of each portion of the anterolateral ligament of the knee separately and all of the portions together in 30 MRI examinations.

Imaging	Tibial portion	Meniscal portion	Femoral portion	Meniscal insertion	Tibial footprint	Femoral footprint
MPR imaging	—	—	—	—	93.33 (28/30)	93.33 (28/30)
CPR imaging	96.67 (29/30)	83.33 (25/30)	90.00 (27/30)	83.33 (25/30)	96.67 (29/30)	96.67 (29/30)
PDW FS	76.67 (23/30)	56.67 (17/30)	73.33 (22/30)	50.00 (15/30)	66.67 (20/30)	16.67 (5/30)
χ^2	5.192	5.079	2.783	7.500	13.127	57.339
p-Value	0.023	0.024	0.095	0.006	0.001	<0.001

MPR, multiplanar reconstruction; CPR, curved planar reconstruction; PDW, proton-density weighted; FS, fat saturation.

MRI scanning technology have been gradually carried out. Klontzas *et al.*[6] used 3D-CISS sequences with MPR to evaluate the ALL and describe the relationship between the ALL and LCL, but did not show more details about the ALL. The CISS sequences are based on the sequence of double-inspired balance steady state-free precession (Balance-SSFP). The CISS adopts two radio frequency excitations with different phase-coding directions, and then two sets of true fast imaging with steady procession (True-FISP) are obtained. Striated artefacts can be removed when the two sets True-FISP are superimposed. The 3D-CISS sequences have been used to evaluate fine structures, such as cranial nerves, and to evaluate ACL healing following surgery. Beyond that, the 3D-CISS sequences with rotating CPR imaging showed more details of the ALL.

In the current study, the visibility of each part on rotating CPR imaging was superior to the visibility on MPR and PDW FS imaging. The result was in agreement with the Helito *et al.* study.[7] The oblique course of the ALL decreased the percentage viewing of each portion of the ALL in only one plane. The 3D-CISS sequences showed anatomic details of the ALL, such as the direction of the fibres. Rotating the CPR technique can uncurl tortuous structures on different plane, so that the structures can be visualised on single or several images. The MPR of 3D-CISS sequences imaging had low sensitivity to distinguish each part and section of the ALL. In the current study, the visibility of each part of the ALL could not be recorded well.

The MPR of the 3D-CISS sequences imaging had low sensitivity to distinguish each part and section of the ALL. In the current study, the visibility of each part of the ALL could not be recorded well. The MPR of the 3D-CISS sequences imaging show the femoral and tibial footprints of the ALL with visibility of 93.3% and 93.3%, respectively. In response to the low percentage of each portion of the MPR viewed, several reasons existed: (1) the oblique course of the ALL decreased the percentage view of each portion of the ALL in only one plane; (2) each portion of the ALL was distinguished on oblique sagittal imaging of the MPR; (3) all portions of the ALL were not visible simultaneously on a single imaging, whether or not oblique coronal or sagittal imaging; and (4) MPR is commonly used for planar cross-section re-sampling from a volumetric data set. The study was the first to measure the angle between the ALL and LCL (18.34±1.88°; range, 13.5–21°) on the MPR of the 3D-CISS sequences imaging. This angle can further show the features of the ALL and LCL. Further research will be needed to show the shape of the ALL on routine 2D images.

Although valuable conclusions were obtained, there were some limitations of the present study, as follows: (1) an inadequate number of volunteers in the study; (2) lack of CISS sequences for some patients; and (3) post-processing was more difficult because of the structure of the ALL.

In conclusion, 3D-CISS sequences with MPR and rotating CPR show more anatomical detail of the ALL and provide more valuable images for clinical diagnosis.

Conflict of interest

The authors declare no conflict of interest.

References

1. Vasilevska Nikodinovska V, Gimber LH, Hardy JC, *et al*. The collateral ligaments and posterolateral corner: what radiologists should know. *Semin Musculoskelet Radiol* 2016;**20**(1):52–64.
2. Vieira EL, Vieira EA, da Silva RT, *et al*. An anatomic study of the iliotibial tract. *Arthroscopy* 2007;**23**(3):269–74.
3. Kosy JD, Mandalia VI, Anaspure R. Characterization of the anatomy of the anterolateral ligament of the knee using magnetic resonance imaging. *Skeletal Radiol* 2015;**44**(11):1647–53.
4. Taneja AK, Miranda FC, Braga CA, *et al*. MRI features of the anterolateral ligament of the knee. *Skeletal Radiol* 2015;**44**(3):403–10.
5. Helito CP, Helito PV, Costa HP, *et al*. MRI evaluation of the anterolateral ligament of the knee: assessment in routine 1.5-T scans. *Skeletal Radiol* 2014;**43**(10):1421–7.
6. Klontzas ME, Maris TG, Zibis AH, *et al*. Normal magnetic resonance imaging anatomy of the anterolateral knee ligament with a T2/T1-weighted 3-dimensional sequence: a feasibility study. *Can Assoc Radiol J* 2016;**67**(1):52–9.
7. Helito CP, Bonadio MB, Soares TQ, *et al*. The meniscal insertion of the knee anterolateral ligament. *Surg Radiol Anat* 2016;**38**(2):223–8.
8. Helito CP, Demange MK, Helito PV, *et al*. Evaluation of the anterolateral ligament of the knee by means of magnetic resonance examination. *Rev Bras Ortop* 2015;**50**(2):214–9.
9. Van Dyck P, Clockaerts S, Vanhoenacker FM, *et al*. Anterolateral ligament abnormalities in patients with acute anterior cruciate ligament rupture are associated with lateral meniscal and osseous injuries. *Eur Radiol* 2016;**26**(10):3383–91.
10. Macchi V, Porzionato A, Morra A, *et al*. The anterolateral ligament of the knee: a radiologic and histotopographic study. *Surg Radiol Anat* 2016;**38**(3):341–8.
11. Claes S, Vereecke E, Maes M, *et al*. Anatomy of the anterolateral ligament of the knee. *J Anat* 2013;**223**(4):321–8.
12. Vincent JP, Magnussen RA, Gezmez F, *et al*. The anterolateral ligament of the human knee: an anatomic and histologic study. *Knee Surg Sports Traumatol Arthrosc* 2012;**20**(1):147–52.
13. Dodds AL, Halewood C, Gupte CM, *et al*. The anterolateral ligament: anatomy, length changes and association with the Segond fracture. *Bone Jt J* 2014;**96-B**(3):325–31.
14. Helito CP, Demange MK, Bonadio MB, *et al*. Anatomy and histology of the knee anterolateral ligament. *Orthop J Sports Med* 2013;**1**(7). 2325967113513546.

15. Caterine S, Litchfield R, Johnson M, *et al*. A cadaveric study of the anterolateral ligament: re-introducing the lateral capsular ligament. *Knee Surg Sports Traumatol Arthrosc* 2015;**23**(11):3186–95.
16. Claes S, Bartholomeeusen S, Bellemans J. High prevalence of anterolateral ligament abnormalities in magnetic resonance images of anterior cruciate ligament-injured knees. *Acta Orthop Belg* 2014;**80**(1):45–9.
17. Helito CP, Helito PV, Bonadio MB, *et al*. Correlation of magnetic resonance imaging with knee anterolateral ligament anatomy: a cadaveric study. *Orthop J Sports Med* 2015;**3**(12). 2325967115621024.
18. Porrino Jr J, Maloney E, Richardson M, *et al*. The anterolateral ligament of the knee: MRI appearance, association with the Segond fracture, and historical perspective. *AJR Am J Roentgenol* 2015;**204**(2):367–73.